Title: The influence of movement on the localization precision of sub-resolution particles in fluorescence microscopy

Authors: H. Deschout, Kristiaan Neyts, K. Braeckmans

In: Journal of Biophotonics, 5(1), 97-109 (2012)

Journal of Biophotonics header will be provided by the publisher

The influence of movement on the localization precision of sub-resolution particles in fluorescence microscopy

Hendrik Deschout [1,2], *Kristiaan Neyts* [3,4], *and Kevin Braeckmans* [*,1,2]

[1] Biophotonic Imaging Group, Laboratory of General Biochemistry and Physical Pharmacy, Ghent University, Harelbekestraat 72, B-9000 Gent, Belgium
[2] Center for Nano- and Biophotonics, Ghent University, Harelbekestraat 72, B-9000 Gent, Belgium
[3] Liquid Crystals & Photonics Group, ELIS Department, Ghent University, Sint-Pietersnieuwstraat 41, B-9000 Gent, Belgium
[4] Center for Nano- and Biophotonics, Ghent University, Sint-Pietersnieuwstraat 41, B-9000 Gent, Belgium

Received zzz, revised zzz, accepted zzz
Published online zzz

Key words: fluorescence microscopy, video microscopy, diffusion, time-lapse imaging, single molecule imaging, single particle tracking, superresolution

Obtaining sub-resolution particle positions in fluorescence microscopy images is essential for single particle tracking and high-resolution localization microscopy. While the localization precision of stationary single molecules or particles is well understood, the influence of particle motion during image acquisition has been largely neglected. Here, we address this issue and provide a theoretical description on how particle motion influences the centroid localization precision, both in case of 2-D and 3-D diffusion. In addition, a novel method is proposed, based on dual-channel imaging, for the experimental determination of the localization precision of moving particles. For typical single particle tracking experiments, we show that the localization precision is approximately two-fold worse than expected from the stationary theory. Strikingly, we find that the most popular localization method, based on the fitting of a Gaussian distribution, breaks down for lateral diffusion. Instead, the centroid localization method is found to perform well under all conditions.

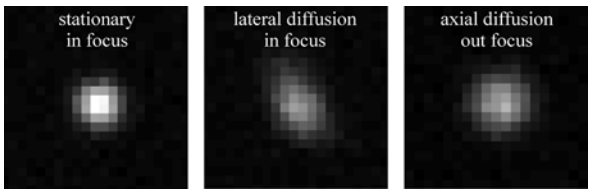

Particle diffusion during image acquisition causes deformation and broadening of the observed intensity distribution in case of lateral and axial diffusion, respectively. This leads to a substantial deterioration of the particle localization precision compared to the stationary case.

1. Introduction

A fundamental property of imaging a point-like object with any optical set-up is that the observed spot has a certain spatial intensity distribution known as the point spread function (PSF). The radial and axial extent of the PSF determines the imaging resolution, which is around 250 nm and 900 nm, respectively, for a research grade epi-fluorescence microscope [1]. Despite the limited spatial resolution, the position of such a small object can be determined with much better precision by locating the

* Corresponding author: e-mail: Kevin.Braeckmans@UGent.be, Phone: +32 9 264 80 78, Fax: +32 9 264 81 89

center point of the PSF. This is an important trick that is applied extensively in single particle/molecule tracking (SPT/SMT) microscopy [2-4], in sub-resolution imaging techniques, such as STORM or PALM [5,6], and a combination thereof [7].

It is, therefore, of great interest to have a detailed knowledge of the different parameters that determine the localization precision. Independent of the method that is used for determining the PSF center position, it was shown that the theoretical lower limit for the localization precision of a stationary particle scales inversely with the square root of the number of detected photons [8,9]. While this result corroborates the common knowledge that as many photons as possible should be collected, there are two other important factors that determine the localization precision. First, due to the fact that images are recorded with a finite pixel size, the sampling of the PSF is not perfect. Secondly, a certain amount of background will usually be present as well. Thompson et al. gave the first approximate theoretical description taking all three factors into account for the case of a stationary particle whose position is determined by the least-squares fitting of a circular 2-D Gaussian function to the PSF in the focal plane [10]. By a more rigorous theoretical derivation, an important correction to this often used equation was recently published by Mortensen et al. [11]. In addition, they provided similar formulas for a fitting algorithm based on maximum likelihood estimation and for more complicated PSF models that describe the dipole emission of single fluorescent molecules. A different way to obtain the particle position, although used less often, is calculating the intensity weighted center position of the PSF spot, also known as the centroid [12,13].

While a sound theoretical basis now exists for the localization precision of stationary particles, the case of moving particles, which is ubiquitous in SPT/SMT experiments, has been largely neglected. Particle movement during image acquisition alters the shape of the observed intensity distribution compared to the stationary PSF, so the localization precision can be expected to be substantially affected. One recent study gives a theoretical treatment of the influence of the special cases of linear and circular movement during image acquisition on the localization precision [14]. However, on a molecular scale, stochastic motion is much more common and of practical relevance. In this case, the observed intensity distribution does not necessarily have a symmetric shape, rendering the popular Gaussian approximation problematic. It should be noted that the effect of particle diffusion during image acquisition was already studied on the level of motion quantification in SPT experiments. A correction on the classical expression for the mean squared displacement (MSD) was proposed, but the influence on the localization precision was not considered [15-18].

In this study, we address the important but currently unanswered question of how 2-D or 3-D stochastic motion influences the localization precision of sub-resolution particles. It is shown that the centroid localization algorithm is the most robust one in the case that the particles move substantially during image acquisition. Therefore, a formula that describes the centroid localization precision in case of 2-D and 3-D stochastic motion is derived. Our theory is validated both by computer simulations as well as experiments by using a novel procedure based on SPT in two different (spectral) channels. It is shown that particle movement can significantly affect the localization precision for all image acquisition times. Furthermore, the centroid estimator is compared to the popular method of least-squares fitting of a circular 2-D Gaussian distribution. Notably, we find that the localization precision for the Gaussian least-squares fitting rapidly deteriorates for increasing image acquisition times. Instead, the much simpler and faster centroid algorithm is found to give a superior localization precision if all pixels that belong to the particle intensity distribution are included.

2. Theory

2.1 Localization precision of diffusing particles

The position of stationary sub-resolution particles in microscopy images is usually estimated by determining the center location of the particle PSF. If multiple images of the same particle are recorded, its apparent center position will be slightly different in each image due to a limited signal-to-noise ratio (SNR). The precision σ with which a particle can be localized, can be defined as the standard deviation on these apparent center positions. According to the Fisher information theory, this precision is fundamentally limited according to [19]:

$$\sigma \geq \frac{\lambda}{2\pi n\sqrt{N}}, \tag{1}$$

with λ the photon wavelength, n the refractive index and N the total number of collected photons. This limit is fundamental, not only because it assumes an ideal noiseless detection process and an infinitely small pixel size, but also because it is independent of the type of PSF center estimator. In real situations, the precision will be worse compared to the limit provided in Eq. (1). The most frequently used method to identify the PSF center location $\vec{r}_p = (x_p, y_p)$ in the focal plane (xy-plane), is the least-squares fitting of a circular 2-D Gaussian distribution to the observed PSF:

$$I(x,y) = \frac{N}{2\pi s^2} e^{-\frac{(x-x_p)^2+(y-y_p)^2}{2s^2}} + B, \tag{2}$$

with s the standard deviation of the Gaussian distribution and B a constant background. Note that this is only an approximate description, the more exact description of the PSF is an Airy distribution with an infinite standard deviation [20]. Arguably, the popularity of this method is due to the frequently cited work of Cheezum et al., where it was argued that this algorithm performs best in low SNR situations, as is often the case in SPT or nanoscopy experiments [21]. An approximate model for the localization precision σ_g of this method was put forward by Thompson et al. in 2002, which was refined by a more rigorous mathematical derivation by Mortensen et al. in 2010 [22,23]:

$$\sigma_g^2 = F\left\{\frac{16\left(s^2 + a^2/12\right)}{9N} + \frac{8\pi b^2\left(s^2 + a^2/12\right)^2}{a^2N^2}\right\}, \quad (3)$$

with a the pixel size and b the background. We will only consider a Poisson distributed photon background, which means that b can also be interpreted as the background standard deviation. The factor F is equal to 1 in case of a CCD or CMOS detector, while it is equal to 2 for an electron multiplying CCD (EMCCD) camera [24-26].

A different type of estimator for the PSF center is the well-known centroid [27]:

$$x_p = \frac{\sum_{i,j}\left(I_{i,j} - B\right)x_{i,j}}{\sum_{i,j}\left(I_{i,j} - B\right)} \quad \text{and} \quad y_p = \frac{\sum_{i,j}\left(I_{i,j} - B\right)y_{i,j}}{\sum_{i,j}\left(I_{i,j} - B\right)}. \quad (4)$$

The sum goes over all the pixels (i, j) that belong to the particle PSF, with $I_{i,j}$ the intensity and $\vec{r}_{i,j} = (x_{i,j}, y_{i,j})$ the pixel coordinate. Similar to Eq. (3) for the Gaussian fitting method, it is possible to derive an expression for the centroid localization precision σ_c of a stationary subresolution particle (see Supporting Material):

$$\sigma_c^2 = F\left\{\frac{s^2 + a^2/12}{N} + \frac{81\pi b^2\left(s^2 + a^2/12\right)^2}{4a^2N^2}\right\}, \quad (5)$$

This expression is valid on condition that all relevant pixels belonging to the particle intensity distribution are included in the centroid calculation, see Eq. (4), while the background is excluded.

Now, we consider the effect of random motion on the localization precision. If a particle is diffusing during image acquisition, the shape of the observed intensity distribution will be significantly distorted compared to the stationary PSF. In case of movement inside the focal plane, the intensity distribution can even become asymmetrical. Fitting of a circular Gaussian function, therefore, does not seem to be a suitable approach (as will be demonstrated in the Results section). Instead, if all relevant pixels are taken into account, the centroid algorithm does not make any assumption on the shape of the intensity distribution and is expected to be a better estimator in case of particle motion. We, therefore, expand the theory of the centroid precision to include particle diffusion during image acquisition. It is important to realize that the centroid is the intensity weighted center, which corresponds to the *average* particle position during the time over which the image is acquired. Furthermore, it should be noted that it is impossible to determine the localization precision of an individual diffusing particle, since its trajectory is unknown and unpredictable by definition. Instead, it is rather the effect on a large ensemble of particles that can be described, i.e. the localization precision that is expected *on average* given a certain diffusion rate and image acquisition time. Since we will investigate 3-D diffusion, the PSF should be considered in 3-D. In extension of the circular 2-D Gaussian PSF for a particle in focus (see Eq. (2)), the fundamental Gaussian beam solution can be used to describe its intensity distribution in a region near the focal plane [28]:

$$I_{gbs}\left(x, y\right) = \frac{N}{2\pi s^2\left(z_p\right)} e^{-\frac{\left(x-x_p\right)^2 + \left(y-y_p\right)^2}{2s^2\left(z_p\right)}}, \quad (6)$$

with the Gaussian standard deviation $s(z_p)$ defined by:

$$s^2\left(z_p\right) = s_0^2\left(1 + \frac{z_p^{\,2}}{z_0^2}\right), \quad (7)$$

where s_0 is the Gaussian standard deviation in the focal plane and $z_0 = (4\pi n/\lambda)s_0^{\,2}$. It should be noted that at a certain distance from the focal plane (e.g. in the order of µm), the PSF shape becomes more complicated and the fundamental Gaussian beam solution is not valid anymore. From a rigorous mathematical derivation (see Supporting Material), it follows that the apparent PSF of particles undergoing lateral diffusion in the focal plane only (i.e. diffusion in the xy-plane, see Figure 1 (A)) can on average still be approximated by a circular 2-D Gaussian distribution with variance:

$$s_{xy}^2 = s_0^2 + \frac{1}{3}D\Delta t, \quad (8)$$

with D the diffusion coefficient and Δt the image acquisition time. A similar but slightly different correction was already proposed by Michalet et al. [29]. However, they performed their calculations assuming that the initial position of the particle during image acquisition is known. In experimental images, this is not the case and it is rather the average position during image acquisition which can be estimated. It is this consideration that leads to the factor 1/3 in Eq. (8), which was omitted in the work by Michalet et al. For particles diffusing in the axial direction along the optical axis (diffusion along the z-axis, see Figure 1 (B)), a detailed calculation shows that the apparent PSF can also be described on average by a circular 2-D Gaussian distribution with variance (see Supporting Material):

$$s_z^2 = s_0^2 + \left(\frac{z_{\lim}^2}{3z_0^2} + \frac{D\Delta t}{3z_0^2}\right)s_0^2, \quad (9)$$

where the average position during the image acquisition time is restricted between the boundaries $z = -z_{\lim}$ and $z = z_{\lim}$ along the optical axis, an assumption based on the apparent PSF becoming indistinguishable from the background if the particle is located too far from the focal plane. In order to reasonably estimate $z_{\lim}$, it can be assumed that a particle becomes undetectable if its peak intensity drops to e^{-2} times its peak intensity in the focal plane, leading to (see Supporting Material):

$$z_{\lim} = z_0\sqrt{e^2 - 1}. \tag{10}$$

In reality, $z_{\lim}$ will depend not only on the optical properties of the objective lens, but also on the particle SNR and image processing settings for detecting the particles. We recently worked out a theoretical framework that allows to accurately determine $z_{\lim}$ from SPT images of 3-D diffusing particles [30]. For clarity, however, in this work we have consistently used Eq. (10), since it was sufficiently accurate for this purpose. Equations (8) and (9) show that both the diffusion in the focal plane and along the optical axis result in an apparent PSF that has on average a circular 2-D Gaussian distribution, with a variance that increases linearly with the image acquisition time and diffusion coefficient:

$$s^2 = s_0^2 + \left(\frac{z_{\lim}^2}{3z_0^2} + \frac{D\Delta t}{3z_0^2}\right)s_0^2 + \frac{1}{3}D\Delta t. \tag{11}$$

For a stationary particle ($D = 0$) that is observed in the focal plane ($z_{\lim} = 0$), we find that $s = s_0$, as expected. Substituting Eq. (11) in Eq. (5), we propose the following description of the average localization precision for centroids, corrected for the influence of 3-D diffusion during image acquisition:

$$\sigma_c^2 = F\frac{s_0^2 + \left(\frac{z_{\lim}^2}{3z_0^2} + \frac{D\Delta t}{3z_0^2}\right)s_0^2 + \frac{1}{3}D\Delta t + \frac{a^2}{12}}{N} + F\frac{81\pi b^2\left(s_0^2 + \left(\frac{z_{\lim}^2}{3z_0^2} + \frac{D\Delta t}{3z_0^2}\right)s_0^2 + \frac{1}{3}D\Delta t + \frac{a^2}{12}\right)^2}{4a^2N^2}. \tag{12}$$

The average localization precision of diffusing particles is thus equal to the localization precision for a PSF blurred by the average diffusion.

2.2 Experimental determination of the localization precision of moving particles

Not only a theoretical description of the localization precision, but also a method that allows experimental determination of this value is of interest. It is well-known that the MSD of a the 2-D trajectory of a diffusing particle is given by [31-35]:

$$MSD = 4Dt - \frac{4}{3}D\Delta t + 4\sigma^2, \tag{13}$$

with t the time interval between the positions in the trajectory (determined by the camera frame rate). When a particle is stationary ($D = 0$), the localization precision σ can be easily determined experimentally by making images of that particle at sequential time points. The MSD of the apparent particle trajectory is then equal to $4\sigma^2$. We will refer to this method as the *single-channel method*, as opposed to the *dual-channel method* for moving particles, which will be explained below. For a moving particle, Eq. (13) suggests that σ could be determined from the intercept of the MSD plot, by fitting of a straight line. However, in reality, one typically has to deal with relatively short trajectories so that, according to our experience, the localization precision cannot be accurately determined this way. Instead, we have developed a novel method, based on SPT in two channels, to determine the localization precision reliably. These can be spectrally different channels (e.g. green and red fluorescence by using a dichroic mirror), but also the same image that is acquired on two detectors (e.g. by using a 50/50 mirror). Consider a particle that is imaged simultaneously in two different channels A and B. The observed trajectories of the particle are described by the positions $\vec{r}_{A,i}$ and $\vec{r}_{B,i}$ (with $i = 1, 2,\ldots$) in channel A and B, respectively (see Figure 2). These positions can be assumed to be distributed around the true particle positions $\vec{r}_{p,i}$. We will consider only the x-dimension, since the same reasoning applies to the y-dimension. The precisions corresponding to the particle locations $x_{A,i}$ and $x_{B,i}$ are defined as σ_A and σ_B, respectively. If the photons in both channels are detected independently from each other, the standard deviation of the differences $x_{A,i} - x_{B,i}$ between the positions in both channels is given by:

$$\sigma_{A-B} = \sqrt{\sigma_A^2 + \sigma_B^2}. \tag{14}$$

In addition, there might be an error on the overlay of the images of both channels, which can be taken into account by introducing an extra overlay contribution σ_o [36]:

$$\sigma_{A-B} = \sqrt{\sigma_A^2 + \sigma_B^2 + \sigma_o^2}. \tag{15}$$

If a 50/50 mirror is used, σ_A and σ_B will be equal to each other, immediately resulting in:

$$\sigma_A = \sigma_B = \sqrt{\frac{\sigma_{A-B}^2 - \sigma_o^2}{2}}. \tag{16}$$

If rather a dichroic mirror is used for detection in two spectrally different channels, a correction has to be made for the different wavelengths and intensities in both channels. If we assume in a first approximation that both σ_A and σ_B are described by the photon shot noise according to Eq. (1), their ratio is given by:

$$\frac{\sigma_A}{\sigma_B} = \frac{\lambda_A}{\lambda_B}\sqrt{\frac{N_B}{N_A}}, \tag{17}$$

with λ_A and λ_B the (average) wavelength in channel *A* and *B*, respectively, and N_A and N_B the corresponding number of collected photons. Combining Eq. (17) with Eq. (15) yields:

$$\sigma_A = \sqrt{\frac{\sigma_{A-B}^2 - \sigma_o^2}{1+\left(\frac{\lambda_B}{\lambda_A}\right)^2 \frac{N_A}{N_B}}} \quad \text{and} \quad \sigma_B = \sqrt{\frac{\sigma_{A-B}^2 - \sigma_o^2}{1+\left(\frac{\lambda_A}{\lambda_B}\right)^2 \frac{N_B}{N_A}}}. \qquad (18)$$

For equal intensities and wavelengths Eq. (18) indeed reduces to Eq. (16). In conclusion, by tracking a diffusing particle in two channels and calculating the variance on the difference between the two positions, the effective localization precision in both channels can be readily calculated with the dual-channel method according to Eq. (16) or (18). Note that the dual-channel method does not make any explicit assumption on the type of motion.

3. Materials and methods

3.1 Computer simulated single particle images

The simulations of images of the apparent PSF of diffusing particles were performed in Matlab (MathWorks, Natick, USA). First, the arrival times $t_{A,i}$ and $t_{B,j}$ (i = 1,..., N_A and j = 1,..., N_B) of N_A and N_B detected photons in channel *A* and *B*, respectively, were determined. For an observed photon emission rate r_A and r_B in channel *A* and *B*, respectively, the expected number of photons during image acquisition time Δt is given by $r_A\Delta t$ and $r_B\Delta t$. These are the averages of the Poisson distributions describing the photon numbers in both channels. Two numbers N_A and N_B were generated from these Poisson distributions using the Matlab function *poissrnd*. The arrival times $t_{A,i}$ and $t_{B,j}$ in channel *A* and *B*, respectively, were then determined by generating N_A and N_B random numbers in the interval [0, Δt] using the Matlab function *rand*. The image acquisition times Δt were chosen between 1 and 30 ms and photon emission rates r_A and r_B had the same value of $2 \cdot 10^5$ s^{-1}, in accordance with our experiments.

As a second step, the particle positions $\vec{r}_{p,k} = (x_p(t_k), y_p(t_k), z_p(t_k))$ were calculated at the times $t_k = \{t_{A,i}, t_{B,i}\}$ (k = 1,..., $N_A + N_B$) for channel *A* and *B* together, with diffusion coefficient D = 1 μm^2/s. For 1-D diffusion, the position $x_p(t_k)$ was determined by taking the position $x_p(t_{k-1})$ and adding a distance from the Gaussian diffusion propagator with variance $2D(t_k - t_{k-1})$ using the Matlab function *randn*. The starting position $\vec{r}_{p,0} = (x_{p,0}, y_{p,0}, z_{p,0})$ at time t = 0 was chosen as $x_{p,0} = y_{p,0}$ = 0 and $z_{p,0}$ a random number in the interval $[-z_{\text{lim}}, z_{\text{lim}}]$, with z_{lim} = 1.5 μm. If the average particle position during Δt was located outside these boundaries, the trajectory was discarded from the analysis. Next, in order to apply the single-channel method for determining the localization precision, the average position of all simulated particle trajectories during Δt should be identical. This was achieved by shifting each time the average position of the trajectory to the origin in the center of the image. Subsequently, the trajectory of the particle in channel *A* or *B* was obtained by extracting the positions $\vec{r}_{p,k}$ corresponding to the photon arrival times $t_k = t_{A,i}$ or $t_k = t_{B,j}$, respectively.

The positions $\vec{r}_{p,k}$ represent the real positions of the particle during Δt. The observed photon positions $\vec{r}_k{}'$ for every t_k were obtained from the probability distribution described by the 3-D Gaussian PSF according to Eq. (6), using the Matlab function *randn*. The standard deviation s_0 of the PSF for a stationary particle in the focal plane was taken equal to 0.15 μm. If all photon positions were generated, they were assigned to M x M pixels, with a pixel size of 0.1 μm. Finally, a normally distributed photon background was added, with a variance equal to 500 s$^{-1}\Delta t$, in the same order of magnitude as for the experimental situation. The variance was assumed to increase linearly with Δt, corresponding to our experiments. The resulting matrix was saved as a 16-bit image. For each image acquisition time typically 1000 images were simulated. The overlay error σ_o in the overlap between the images of both channels was taken equal to zero. Once all simulated images were obtained, the image processing software that was used in the actual experiments and described in the Materials and Methods section and Supporting Material, was used to identify and localize the particles.

3.2 Experimental set-up

The SPT experiments were carried out on a custom-built laser widefield epi-fluorescence microscope set-up that is described elsewhere in more detail [37]. Briefly, two solid state lasers were used for illumination: a 100 mW Calypso 491 nm (Cobolt, Solna, Sweden) and a IQ1C 30 mW 636 nm (Power Technology, Little Rock, USA). The microscope was a Nikon TE2000-E (Nikon Belux, Brussels, Belgium) with a Nikon Plan Apochromat 100× NA1.4 oil immersion objective lens. The fluorescence light coming from the sample was collected again by the objective lens and sent through the side port of the microscope towards the Cascade II:512 EMCCD camera (Roper Scientific, Tucson, USA). A pair of achromat lenses was placed in between the camera and microscope side port for an extra 2× magnification of the image on the CCD chip so that one pixel corresponded to a distance of 89 nm in the sample. A dichroic mirror placed between both achromat lenses reflected the fluorescent light with a wavelength below 560 nm and transmitted the wavelengths above 560 nm. Accompanying mirrors and notch filters (AHF Analysentechnik, Tübingen, Germany) guided the reflected and transmitted part of the fluorescence each to one half of the CCD chip. High-

speed movies were recorded using the Nikon Elements R imaging software. The camera does not output photon numbers but pixel values in analogue-to-digital units that are linearly related to the number of photons collected by the pixels. The conversion factor, which is called the gain, was calibrated with the method published by Janesick [38], using the intensity average and variance from both a dark and an even illuminated image, for an electron multiplication factor that was kept constant throughout the experiments.

3.3 Sample preparation and experimental protocol

SPT experiments were performed on 200 nm diameter Tetraspeck polystyrene nanospheres (Invitrogen, Merelbeke, Belgium), containing, among other fluorescent labels, a green (505 nm excitation peak, 515 nm emission peak) and a red (660 nm excitation peak, 680 nm emission peak) fluorescent label. The fluorescence emission of the green and red label was detected each on a separate half of the CCD chip to enable simultaneous dual-color imaging. The beads were diluted in water to a concentration of approximately 10^9 particles per ml. A microscope sample was prepared by applying 5 µl of the bead suspension between a microscope slide and a cover glass with a double-sided adhesive Secure-Seal Spacer of 120 µm thickness (Molecular Probes, Leiden, The Netherlands) in between. To obtain a sample with stationary particles, 5 µl (with typical concentration of 10^8 particles per ml) was applied on the cover slip and allowed to evaporate, leaving only the nanospheres behind. A microscope sample was prepared by applying 5 µl of water on top of the beads, and the sample was sealed with a cover glass using the double-sided adhesive Secure-Seal Spacer. To increase the camera frame rate, a subregion of the CCD chip of 256 by 512 pixels was selected. Typical image acquisition times were between 1 and 32 ms per frame, with a corresponding frame rate of about 20 to 40 frames per second. For each sample typically 20 movies of about 10 s were recorded at different locations within the sample, with about 20 to 100 particles detected in each movie.

3.4 Single particle tracking data analysis

In case of experimental data, the images from both channels were first aligned, making use of an affine transformation with parameter values derived from an image with stationary multi-color particles. This procedure resulted in an average overlay precision σ_o of approximately 3 nm over the entire field of view, as obtained from Eq. (15) with $\sigma_{A\text{-}B}$ the standard deviation of the differences between the positions of the same particle in both channels and σ_A and σ_B the localization precisions in both channels separately.

Analysis of the experimental and simulated SPT images was performed in Matlab with custom image processing software for identifying and tracking of the individual particles, as explained in more detail in the Supporting Material and elsewhere [31]. For each identified particle, a contour that circumscribes the intensity distribution was calculated. We would like to note that these contours do not have a predefined shape. The centroid was calculated for each particle using the pixels within the contour, taking into account the local background intensity.

As indicated in the Results section, in some cases a circular and elliptical 2-D Gaussian function was least-squares fitted (without weighting) to each particle intensity distribution, yielding the Gaussian center positions. The full variation of shapes (two different standard deviations and the orientation) was included in the fit of the elliptical 2-D Gaussian function, see Eq. (42) in the Supporting Material.

3.5 Calculation of the theoretical localization precision

In order to use Eq. (5) for the determination of the localization precision of stationary particles, several parameters had to be determined. Since an EMCCD camera was used, the factor F was taken equal to 2. The number of photons N could be obtained from the particle spot intensities (i.e. the pixel values within the contour) and was found to be on average $1.97 \cdot 10^5\ s^{-1}\Delta t$ in the green channel and $2.01 \cdot 10^5\ s^{-1}\Delta t$ in the red channel. The PSF standard deviation s_0 was determined to be 0.143 µm in the green and 0.157 µm in the red channel. The photon background variance was estimated from the experimental SPT movies as $54\ s^{-1}\ \Delta t$ in the green and $25\ s^{-1}\ \Delta t$ in the red channel. Note that this variance is equal to Fb^2 instead of b^2 in Eq. (5), considering the electron multiplication process of the EMCCD camera.

In case of diffusing particles, the theoretical localization precision was calculated from Eq. (12) (with F equal to 2). The number of photons N was found to be on average $0.98 \cdot 10^5\ s^{-1}\Delta t$ in the green channel and $0.72 \cdot 10^5\ s^{-1}\Delta t$ in the red channel. The photon background variance Fb^2 was estimated from the experimental SPT movies as $184\ s^{-1}\ \Delta t$ in the green and $78\ s^{-1}\ \Delta t$ in the red channel. The diffusion coefficient was calculated from least-squares fitting Eq. (13) to the mean squared displacements of the particle trajectories. Only the displacements corresponding to the first 25% of the time lags were included, with the localization precision as a free parameter, resulting in an average diffusion coefficient D of 1.6 $\mu m^2/s$ [39].

Weights were added to the least-squares fitting according to the theory from Qian et al. [40]. The maximum detection distance from the focal plane z_{lim}, estimated from Eq. (10), was found to be around 1.66 µm and 1.82 µm in the green and red channel, respectively.

4. Results

4.1 Simulations

A first validation of the theory for determining the localization precision of diffusing particles, as well as the experimental dual-channel method, was performed using computer simulated images of diffusing sub-resolution particles. For several acquisition times, images of the PSF of stationary and diffusing particles were simulated. Subsequently, the particle locations in these simulated images were obtained by the centroid algorithm, and additionally also by least-squares fitting of the circular and elliptical 2-D Gaussian functions. Since the average particle position in the simulated images is located in the origin, the classic single-channel method could also be used to determine the localization precision in case of the diffusing particles, allowing validation of the theory. This would not have been possible for experimental images of a moving particle whose trajectory, and hence time-averaged position, during image acquisition is variable and unknown a priori. All images were simulated in two channels with equal wavelength and equal intensity, to validate the dual-channel method by comparison with the single-channel method.

As can be seen in Figure 3 (A), for each PSF center estimator, the localization precision decreases with the image acquisition time, as expected for stationary particles. Both least-squares methods result in approximately the same localization precision, which is in excellent agreement with the theory of Mortensen et al., see Eq. (3) (with $F = 1$). The localization precision of the centroid method performs nearly identical as well. To investigate the effect of diffusion during acquisition, images were simulated for a particle diffusing with a diffusion coefficient of 1 $\mu m^2/s$ for different image acquisition times. First, the particle was allowed to move along the *z*-direction only, obtaining the situation of axial diffusion along the optical axis. As can be seen from the results in Figure 3 (B), the three PSF center estimators produced nearly identical results in this case. For all acquisition times, the localization precision becomes > 80% worse compared to the stationary theory of Mortensen et al. The effect of lateral diffusion, i.e. movement restricted to the *xy*-plane, on the localization precision is shown in Figure 3 (C). In this situation, the three estimators behave quite differently from each other. The centroid precision becomes only slightly worse than the stationary case with increasing image acquisition times. Strikingly, however, the precision of both least-squares fits rapidly deteriorates for longer image acquisition times. Fitting of the elliptical 2-D Gaussian function (see Supporting Material) results in a localization precision that is somewhat better than for the circular symmetric 2-D Gaussian, but is still much worse than the centroid method. When the particle is diffusing in all 3 dimensions, a combination of the behavior in the axial and lateral diffusion case can be seen for the three estimators in Figure 3 (D). We can conclude that the centroid estimator has the best overall performance in case of particle diffusion, while the Gaussian fitting methods rapidly break down for lateral diffusion in case of longer image acquisition times.

We have used the centroid data of the diffusing particles, obtained with the single-channel method, to validate Eqs. (5) and (12) (with $F = 1$) which we derived in the Theory section. As can be seen from Figure 4 (A), the theory accurately describes the behavior of the centroid precision in case of stationary particles. In the case of axial diffusion, the correction from Eq. (9) nicely accounts for the > 80% decrease in precision, as can be seen from Figure 4 (B). The small decrease in centroid precision for larger image acquisition times, if the particle is laterally diffusing, is captured well by the correction from Eq. (8), as demonstrated in Figure 4 (C). Also in case of 3-D diffusion, we now see a very good correspondence between theory and simulated data (see Figure 4 (D)). From the results in Figure 4, it can be seen that the centroid precision theory slightly underestimates the simulated values (typically less than 10%, which is less than 2 nm in absolute terms). A hypothesis for this deviation is provided in the Discussion section.

We performed similar simulations for two detection channels as well, allowing to validate the new dual-channel method that we put forward for the experimental determination of the localization precision of diffusing particles. As can be seen from Figure 4, the precision values of the dual-channel method correspond well to the values from the classic single-channel method, demonstrating the validity of this method.

4.2 Single particle tracking experiments

Through simulations, we showed that our model accurately describes the localization precision of the centroid algorithm in case of diffusion. In a last step, we wanted to verify this model against experimental data using SPT movies of multi-color fluorescent 200 nm diameter nanospheres that are diffusing in water. To this end, we have developed the dual-channel method that allows to calculate the localization precision of particles that are moving during image acquisition from experimental SPT

images. To apply the dual-channel method, the SPT movies are recorded in two different colors, referred to as the green and red channel.

First, it was checked if the dual-channel method performs correctly on stationary beads in comparison with the classic single-channel method. The dual-channel precision values were obtained for the green and red channel separately using Eq. (18). As can be seen from the results in Figure 5 (A), the single and dual-channel methods are in excellent agreement with each other for the green channel, and both methods are in agreement with the theoretical prediction for stationary particles, see Eq. (5) (with $F = 2$). The same result was found for the red channel (data not shown). We then applied the dual-channel method to the diffusing particles, the results correspond well with the theoretical prediction according to Eq. (12) (with $F = 2$), as shown in Figure 5 (B). Comparison with the theoretical predication that does not take the diffusion into account (Eq. (5) with $F = 2$) shows that the stationary theory underestimates the diffusion localization precision significantly, by roughly a factor of 2, for all image acquisition times, see Figure 5 (B).

5. Discussion

When sub-resolution particles or molecules are localized in microscopy images, typically a theoretical PSF model is fitted to the observed intensity distribution and the real particle position is estimated by the fitted PSF center. This results in a localization precision that is significantly better than the width of the intensity distribution, a property that has been conveniently used for decades in SPT and more recently in nanoscopy methods based on fluorophore localization [3,41,42]. Up to now, most efforts in estimating this localization precision explicitly or implicitly assume that the particle is immobile during image acquisition [43-45]. This is a reasonable assumption, because strictly speaking the location of a mobile particle during the image acquisition time cannot be defined. Nonetheless, moving particles have an average position during image acquisition, and localization of this average position is possible. Particle movement, however, affects the observed intensity distribution so that the localization precision for moving particles can be expected to be significantly worse compared to the stationary case. In recent work, the effect of a priori known linear and circular motion on the localization precision was studied within the framework of the Fisher information theory [46,47]. We, on the other hand, have considered stochastic motion, which is more relevant on the molecular scale. Since, to the best of our knowledge, stochastic motion is not easily implemented in the Fisher information approach, we have expanded the popular existing theories on stationary particle localization to include the effects of 2-D and 3-D diffusion during image acquisition.

It is important to realize that, due to the stochastic motion, it is impossible to predict the localization precision of an individual particle. What is possible, though, is to give a description of the *average* localization precision of a large ensemble of particles. The PSF of a stationary sub-resolution particle is often described as a circular 2-D Gaussian distribution. The theory presented in this work, shows that a Gaussian description is *on average* still valid in case of 2-D and 3-D diffusion, but now with a variable standard deviation that depends on the diffusion coefficient and the image acquisition time. Note that it was recently shown that the apparent PSF of a single rotating dipole emitter can be approximated by a Gaussian function, which suggests that the proposed theory of a variable Gaussian variance can also be applied on moving fluorophores with dipole photon emission [48]. For an individual particle, the observed intensity distribution shape can deviate substantially from a circular Gaussian distribution. This explains why we found that determining the position of diffusing particles by the classic Gaussian fitting method ceased to work correctly for longer image acquisition times. The elliptical 2-D Gaussian function could possibly take the spot deformation somewhat better into account. However, our results showed that the localization precision was only slightly improved, compared to the circular 2-D Gaussian. Most likely, this is due to the fact that, compared to the stationary case, the shape of the apparent PSF becomes distorted and asymmetrical in such a way that it starts to exhibit multiple maxima for longer image acquisition times.

The centroid algorithm, which does not rely on any assumption on the shape of the observed intensity distribution, was found to be a superior particle location estimator in case of movement during image acquisition, compared to the least-squares fitting of the 2-D Gaussian. Through a rigorous mathematical derivation, we succeeded in deriving an expression that predicts the centroid localization precision for particles diffusing in the focal plane or even in 3-D. The theory matched almost perfectly with both simulated and experimental particle localization data. It was found that motion along the optical axis decreases the centroid precision nearly independently of the image acquisition time. The lateral motion in the focal plane only affects the centroid precision for long image acquisition times or large diffusion coefficients. For diffusing particles we conclude that the centroid method globally outperforms the much used least-squares fitting of a circular or elliptical Gaussian function. This would appear to be in disagreement with the conclusion put forward in the article by Cheezum et al., who made a systematic comparison between different lo-

calization algorithms [49]. By simulating images of stationary particles, they found that the Gaussian fitting method performed better than the centroid algorithm in low SNR conditions. However, particle motion was not considered, which turns out to be the determining factor for longer image acquisition times.

We would like to note that, although the theory accurately describes the centroid precision, it was derived under the specific assumption that all relevant pixels that contribute to the PSF are included in the centroid calculation, while background pixels should be excluded. Any deviation from this assumption might lead to a decrease in the localization precision compared to what is expected theoretically. We hypothesize that this, at least partially, could explain the small underestimation of the simulated values by the theory that we found. Possibly not all relevant pixels were included by the automated selection procedure, so that somewhat less photons were taken into account, leading to a slightly higher uncertainty on the particle locations as determined from the simulated images. An additional contribution to the experimental localization uncertainty could stem from the fact that a particle is never exactly located at the center of a pixel. As a consequence, when selecting an iso-intensity contour, some more pixels might be included on one side of the center compared to the other side. This in turn can lead to an additional contribution to the error in the determination of the particle location. Nevertheless, if these effects are present, they are in any case quite small considering the excellent agreement between theory and experiment.

Apart from applications in high-resolution localization microscopy (e.g. STORM/PALM), the theory of the localization precision that takes movement during image acquisition into account, can also be used to more precisely determine the diffusion coefficient from the MSD plot. The MSD expression in Eq. (13) for free diffusion contains two important corrections. The first correction comes from the fact that the diffusing particle does not have a unique location during the image acquisition. Instead, the particle location is rather the average position of the particle during the image acquisition time [50-52]. The second correction was investigated in this study and takes into account the finite localization precision, which we have shown to depend on the diffusion coefficient, see Eq. (12). For accurate diffusion measurements we suggest to use Eq. (13) in combination with Eq. (12) for fitting to the MSD curves where D is treated as a free fitting parameter in all three terms. As shown in Figure 3 in the Supporting Material, this allows for a more precise determination of the diffusion coefficient compared to treating the localization uncertainty σ as an entirely free fitting parameter.

A practical consequence of our theory is that it allows to estimate an optimal image acquisition time for a given diffusion coefficient. To this end, it is instructive to write the theoretical centroid precision explicitly as a function of the image acquisition time. It is reasonable to assume that $N = r\Delta t$, meaning that the number of photons N increases linearly with the image acquisition time Δt, with r the observed photon emission rate. The localization precision in Eq. (12) can thus be rewritten as:

$$\sigma_c^2 = F\frac{\left(s_0^2+\frac{z_{\lim}^2}{3z_0^2}s_0^2+\frac{a^2}{12}\right)+\left(\frac{1}{3}+\frac{s_0^2}{3z_0^2}\right)D\Delta t}{r\Delta t} + F\frac{81\pi b^2\left(\left(s_0^2+\frac{z_{\lim}^2}{3z_0^2}s_0^2+\frac{a^2}{12}\right)+\left(\frac{1}{3}+\frac{s_0^2}{3z_0^2}\right)D\Delta t\right)^2}{4a^2r^2\Delta t^2}. \quad (19)$$

The first term always decreases with larger image acquisition times. In a first approximation, we can assume that the background mainly comes from out-of-focus light, so that it is Poisson distributed with variance $b^2 = \beta\Delta t$. This causes the second term in Eq. (19) to increase with larger image acquisition times (see Figure 4 in the Supporting Material), resulting in an optimal localization precision for the following image acquisition time:

$$\Delta t_{\min} = \sqrt{\frac{r\left(s_0^2+\frac{z_{\lim}^2}{3z_0^2}s_0^2+\frac{a^2}{12}\right)+\frac{81\pi}{4a^2}\beta\left(s_0^2+\frac{z_{\lim}^2}{3z_0^2}s_0^2+\frac{a^2}{12}\right)^2}{\frac{81\pi}{4a^2}\beta D^2\left(\frac{1}{3}+\frac{s_0^2}{3z_0^2}\right)^2}} \quad (20)$$

Beyond this point, the localization precision will deteriorate. This minimum, however, is quite weak and only occurs for long image acquisition times, for example around 274 ms for typical parameters values used in our experiments (see Figure 4 in Supporting Material). This would result in very slow frame rates and is therefore not an optimal image acquisition time when studying dynamic events. In practice, one will typically have to make a trade-off between the localization precision and a sufficiently high frame rate, using Eq. (19).

Although only the case of free particle diffusion was treated in the Theory section, one could wonder what the effect would be in case of anomalous sub- or super-diffusion. These types of motion can be described by a Gaussian probability distribution that is similar to the one for free diffusion, but with the diffusion coefficient replaced by a time-dependent variable [3]. However, considering the increased complexity, it is likely not worth the effort, since the image acquisition time is short compared to the time scale over which the MSD curve should be analyzed in order to detect anomalous diffusion. Indeed, for short time lags, the MSD curve is always nearly linear so that it seems sensible to describe

the particle movement by free diffusion during the short image acquisition time.

Besides the theoretical model, also a simple empirical method was presented that allows to experimentally determine the localization precision of moving particles. Usually, the localization precision is calculated experimentally by taking the standard deviation of the positions of the same particle determined at several time points. This approach is valid for stationary particles, but of course not for moving particles whose position is unknown and variable over time. The proposed dual-channel method calculates the localization precision using the standard deviation of the differences between the positions of two trajectories of the same particle, determined simultaneously in two different channels. In this study, we have made use of multi-color beads that are visible in two spectrally different channels. However, it should be noted that this method is not limited thereto, and it is equally possible to make use of e.g. a 50/50 mirror and detect the same image on two detectors (or two halves of a CCD chip as was done here). The only requirement for the dual-channel method to work is that the photons in both channels should be detected independently from each other. Noteworthy, this dual-channel method is not limited to a specific type of motion so that it could be also applied to other types of motion than free diffusion.

6. Conclusion

We have shown that movement during the image acquisition time degrades the precision with which single particles or molecules can be localized. In agreement with our theory, lateral movement in the focal plane was found only to affect the precision for large image acquisition times, while axial movement perpendicular to the focal plane always degraded the precision. Attention should be paid in case of fitting of a Gaussian function, because the deformation of the point spread function caused by lateral movement results in a rapid deterioration of the localization precision. The centroid algorithm does not suffer from this drawback and is, therefore, a more reliable position estimator for moving particles.

Acknowledgements Hendrik Deschout is a doctoral fellow of the Institute for the Promotion of Innovation through Science and Technology in Flanders (IWT), Belgium. Financial support by the Fund for Scientific Research Flanders (FWO) is acknowledged with gratitude. We would like to thank Magnus Röding for help with the statistical analysis of the data.

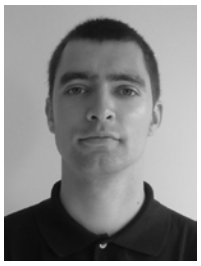

Hendrik Deschout is a PhD student at Ghent University in the Biophotonic Imaging Group hosted by the Laboratory of General Biochemistry and Physical Pharmacy. He obtained a MSc degree in Physics in 2006 and a MSc degree in Engineering Physics in 2008 from Ghent University. His research mainly concerns single particle tracking and other fluorescence microscopy techniques for application in drug delivery research.

Kristiaan Neyts is a full research professor at Ghent University, in the ELIS department of the faculty of Engineering and Architecture. He is heading the Liquid Crystals and Photonics group that is conducting research in the fields of liquid crystals, OLEDs and electrophoresis. This group of 18 researchers has expertise in device technology, numerical simulations and electro-optical characterization. Kristiaan Neyts is co-author of over 100 journal papers listed in the Web of Science. He made his PhD in the field of thin film electroluminescence in 1987 and is now involved in research projects in basic and applied research, in collaboration with universities and companies worldwide. His main research results are in the following fields: light propagation in structured anisotropic media, spatial optical solitons in liquid crystals, light emission from thin film structures and OLEDs, electrophoresis in non-polar media and optics of lighting and displays.

Kevin Braeckmans is a professor at Ghent University, where he is heading the Biophotonic Imaging Group hosted by the Laboratory of General Biochemistry and Physical Pharmacy. He obtained a MSc degree in Physics in 1999, and a PhD in Pharmaceutical Sciences from Ghent University in 2004. Being part of the Center of Nano- and Biophotonics at Ghent University, his research focuses on the development and application of biophotonic imaging techniques for studying biological barriers in drug delivery and for biomedical diagnostics.

References

[1] J. E. N. Jonkman and E. H. K. Stelzer, in: A. Alberto, ed., Confocal and Two-Photon Microscopy : Foundation, Applications, and Advances, (Wiley-Liss, Inc., New York, 2002), pp. 101-126.

[2] V. Levi and E. Gratton, Cell Biochemistry and Biophysics **48**, 1-15 (2007).
[3] M. J. Saxton and K. Jacobson, Annual Review of Biophysics and Biomolecular Structure **26**, 373-399 (1997).
[4] S. Wieser and G. J. Schutz, Methods **46**, 131-140 (2008).
[5] E. Betzig, G. H. Patterson, R. Sougrat, O. W. Lindwasser, S. Olenych, J. S. Bonifacino, M. W. Davidson, J. Lippincott-Schwartz, and H. F. Hess, Science **313**, 1642-1645 (2006).
[6] W. E. Moerner, Proceedings of the National Academy of Sciences of the United States of America **104**, 12596-12602 (2007).
[7] S. Manley, J. M. Gillette, G. H. Patterson, H. Shroff, H. F. Hess, E. Betzig, and J. Lippincott-Schwartz, Nature Methods **5**, 155-157 (2008).
[8] R. J. Ober, S. Ram, and E. S. Ward, Biophysical Journal **86**, 1185-1200 (2004).
[9] N. Bobroff, Review of Scientific Instruments **57**, 1152-1157 (1986).
[10] R. E. Thompson, D. R. Larson, and W. W. Webb, Biophysical Journal **82**, 2775-2783 (2002).
[11] K. I. Mortensen, L. S. Churchman, J. A. Spudich, and H. Flyvbjerg, Nature Methods **7**, 377-U59 (2010).
[12] M. K. Cheezum, W. F. Walker, and W. H. Guilford, Biophysical Journal **81**, 2378-2388 (2001).
[13] R. N. Ghosh and W. W. Webb, Biophysical Journal **66**, 1301-1318 (1994).
[14] Y. Wong, Z. P. Lin, and R. J. Ober, Ieee Transactions on Signal Processing **59**, 895-911 (2011).
[15] M. Goulian and S. M. Simon, Biophysical Journal **79**, 2188-2198 (2000).
[16] X. Michalet, Physical Review e **82**, (2010).
[17] T. Savin and P. S. Doyle, Biophysical Journal **88**, 623-638 (2005).
[18] D. Montiel, H. Cang, and H. Yang, Journal of Physical Chemistry B **110**, 19763-19770 (2006).
[19] R. J. Ober, S. Ram, and E. S. Ward, Biophysical Journal **86**, 1185-1200 (2004).
[20] M. Born and E. Wolf, Principles of optics, (Cambridge University Press, Cambridge, 1999).
[21] M. K. Cheezum, W. F. Walker, and W. H. Guilford, Biophysical Journal **81**, 2378-2388 (2001).
[22] K. I. Mortensen, L. S. Churchman, J. A. Spudich, and H. Flyvbjerg, Nature Methods **7**, 377-U59 (2010).
[23] R. E. Thompson, D. R. Larson, and W. W. Webb, Biophysical Journal **82**, 2775-2783 (2002).
[24] K. I. Mortensen, L. S. Churchman, J. A. Spudich, and H. Flyvbjerg, Nature Methods **7**, 377-U59 (2010).
[25] T. W. Quan, S. Q. Zeng, and Z. L. Huang, Journal of Biomedical Optics **15**, (2010).
[26] M. S. Robbins and B. J. Hadwen, Ieee Transactions on Electron Devices **50**, 1227-1232 (2003).
[27] M. K. Cheezum, W. F. Walker, and W. H. Guilford, Biophysical Journal **81**, 2378-2388 (2001).
[28] A. Yariv, Quantum electronics, (John Wiley & Sons, Inc., New York, 1989).
[29] X. Michalet, Physical Review e **82**, (2010).
[30] M. Röding, H. Deschout, K. Braeckmans, and M. Rudemo, Physical Review e **84**, (2011).
[31] K. Braeckmans, D. Vercauteren, J. Demeester, and S. C. De Smedt, in: A. Diaspro, ed., Nanoscopy and Multidimensional Optical Fluorescence Microscopy, (CRC Press / Taylor & Francis Group, Boca Raton, 2010).
[32] J. C. Crocker and D. G. Grier, Journal of Colloid and Interface Science **179**, 298-310 (1996).
[33] M. Goulian and S. M. Simon, Biophysical Journal **79**, 2188-2198 (2000).
[34] X. Michalet, Physical Review e **82**, (2010).
[35] T. Savin and P. S. Doyle, Biophysical Journal **88**, 623-638 (2005).
[36] I. Koyama-Honda, K. Ritchie, T. Fujiwara, R. Iino, H. Murakoshi, R. S. Kasai, and A. Kusumi, Biophysical Journal **88**, 2126-2136 (2005).
[37] K. Braeckmans, K. Buyens, W. Bouquet, C. Vervaet, P. Joye, F. De Vos, L. Plawinski, L. Doeuvre, E. ngles-Cano, N. N. Sanders, J. Demeester, and S. C. De Smedt, Nano Letters **10**, 4435-4442 (2010).
[38] J. R. Janesick, Scientific Charge-Coupled Devices, (SPIE - The International Society for Optical Engineering, Bellingham, Washington, 2001).
[39] M. J. Saxton, Biophysical Journal **72**, 1744-1753 (1997).
[40] H. Qian, M. P. Sheetz, and E. L. Elson, Biophysical Journal **60**, 910-921 (1991).
[41] E. Betzig, G. H. Patterson, R. Sougrat, O. W. Lindwasser, S. Olenych, J. S. Bonifacino, M. W. Davidson, J. Lippincott-Schwartz, and H. F. Hess, Science **313**, 1642-1645 (2006).
[42] W. E. Moerner, Proceedings of the National Academy of Sciences of the United States of America **104**, 12596-12602 (2007).
[43] K. I. Mortensen, L. S. Churchman, J. A. Spudich, and H. Flyvbjerg, Nature Methods **7**, 377-U59 (2010).
[44] R. J. Ober, S. Ram, and E. S. Ward, Biophysical Journal **86**, 1185-1200 (2004).
[45] R. E. Thompson, D. R. Larson, and W. W. Webb, Biophysical Journal **82**, 2775-2783 (2002).
[46] S. Ram, E. S. Ward, and R. J. Ober, Multidimensional Systems and Signal Processing **17**, 27-57 (2006).
[47] Y. Wong, Z. P. Lin, and R. J. Ober, Ieee Transactions on Signal Processing **59**, 895-911 (2011).
[48] S. Stallinga and B. Rieger, Optics Express **18**, 24461-24476 (2010).
[49] M. K. Cheezum, W. F. Walker, and W. H. Guilford, Biophysical Journal **81**, 2378-2388 (2001).

[50] M. Goulian and S. M. Simon, Biophysical Journal **79**, 2188-2198 (2000).
[51] X. Michalet, Physical Review e **82**, (2010).
[52] T. Savin and P. S. Doyle, Biophysical Journal **88**, 623-638 (2005).

Figures

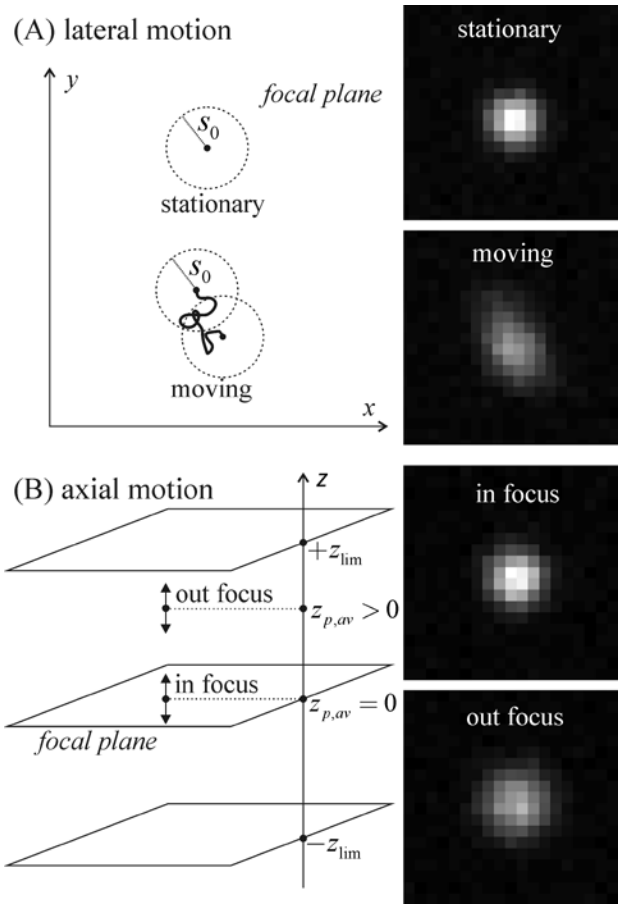

Figure 1 (A) Illustration of the influence of lateral movement parallel to the focal plane on the PSF. Two different situations are shown: a stationary particle and a diffusing particle in the focal plane. The trajectories during the image acquisition time are shown together with their PSF. The circular Gaussian approximation of the stationary PSF has a standard deviation s_0. (B) Illustration of the influence of axial movement perpendicular to the focal plane on the PSF. Two different situations are shown: a particle on average in focus with $z_{p,av} = 0$ and a particle on average out focus with $z_{p,av} > 0$. The PSF of the particle in focus has a smaller standard deviation than the PSF of the particle out focus.

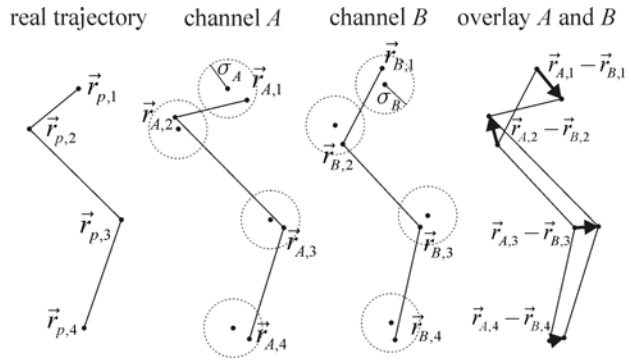

Figure 2 Illustration of the dual-channel method for determining the localization precision of moving particles. The true particle trajectory consists out of 4 positions $\vec{r}_{p,i}$ (i = 1,…,4). The particle positions $\vec{r}_{A,i}$ and $\vec{r}_{B,i}$ that are detected in channel A and B, respectively, are normally distributed around the true position $\vec{r}_{p,i}$ with standard deviations σ_A and σ_B, respectively. Making an overlay of the images in both channels and taking the standard deviation of the difference between the positions $\vec{r}_{A,i}$ - $\vec{r}_{B,i}$ for every i, results in the localization precision σ_A and σ_B.

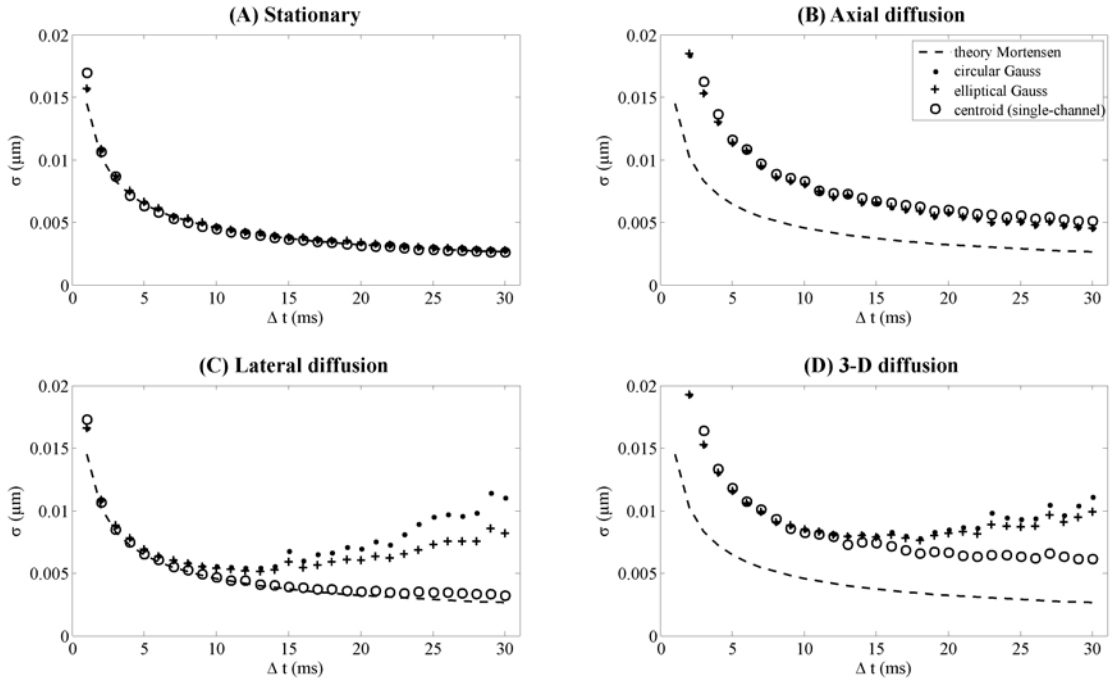

Figure 3 The localization precision, as determined from simulated images, is shown in function of the image acquisition time. The results for 3 different PSF center estimators (the centroid (○) and the least-squares fitting of a circular (•) and elliptical (+) 2-D Gaussian function) are shown in case of: (A) stationary particles, (B) particles diffusing along the axial direction only, (C) particles diffusing in the focal plane only, (D) particles diffusing in 3-D. The dashed line is the same for (A) to (D) and represents the theoretical prediction according to Mortensen et al. for the stationary particles (see Eq. (3) with $F = 1$).

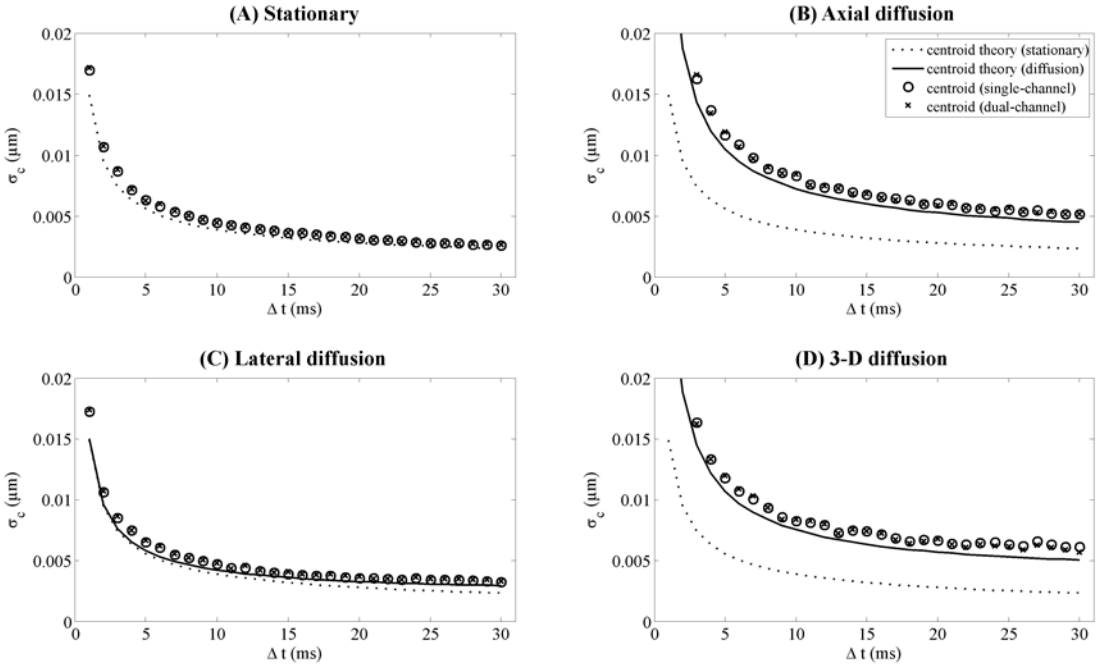

Figure 4 The localization precision, as determined from simulated images, is shown in function of the image acquisition time. The results for the centroid are shown in function in case of: (A) stationary particles, (B) particles diffusing along the axial direction only, (C) particles diffusing in the focal plane only, (D) particles diffusing in 3-D. The centroid precision values obtained by both the single-channel (○) and dual-channel (×) method are shown. The dotted line is the same and represents the theory for the stationary particles (see Eq. (5) with $F = 1$). The full line shows the theory that takes the diffusion (axial, lateral or both) during image acquisition time into account (see Eq. (12) with $F = 1$).

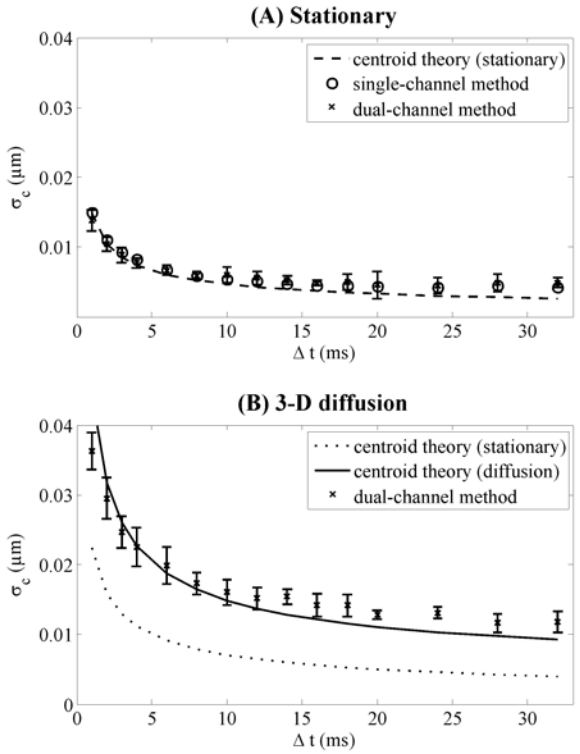

Figure 5 The experimentally determined centroid precision from dual-color SPT movies of stationary and diffusing 200 nm diameter nanospheres is shown in function of the image acquisition time. The results from for the green channel are shown for: (A) the stationary particles and (B) the diffusing particles. For the stationary particles, both the single-channel (○) and dual-channel (×) precision values are shown, for the diffusing particles only the dual-channel (×) values. The error bars represent the 95% confidence intervals of the dual-channel values. The dashed line in (A) shows the theoretical prediction for the stationary particles (see Eq. (5) with $F = 2$). The dotted line in (B) shows the theoretical prediction if the diffusion is not taken into account (see Eq. (5) with $F = 2$). The full line in (B) represents the theoretical prediction that takes the diffusion during image acquisition time into account (see Eq. (12) with $F = 2$).